Journal of Nuclear Materials 409 (2011) 47–52

Contents lists available at ScienceDirect

Journal of Nuclear Materials

journal homepage: www.elsevier.com/locate/jnucmat

Thermodynamic modeling of the Zr–H–Nb system on the Zr-rich side and application

Jianwei Wang [a,*], Lijun Wang [a], Weidong Chen [a], Qian Huang [b], Jianyun Shen [a]

[a] Division of Mineral Resources, Metallurgy and Materials, General Research Institute for Nonferrous Metals, Beijing 100088, PR China
[b] School of Mechanical Electronic and Information Engineer, China University of Mining and Technology, Beijing 100083, PR China

ARTICLE INFO

Article history:
Received 11 November 2010
Accepted 23 December 2010
Available online 29 December 2010

ABSTRACT

A thermodynamic modeling of the Zr–H–Nb system on the Zr-rich side (wt.%Nb $\leqslant$ 2.5) was established using CALPHAD (CALculation of PHAse Diagrams) method. The calculated pressure-composition isotherms and the composition limits in the two-phase (bcc + fcc) region agree well with the experimental data. Meanwhile, some thermodynamic data of Zr–H–Nb system (wt.%Nb = 1, P_{H_2}=101.325 kPa) was calculated, such as equilibrium hydrogen concentration, phase composition and phase transition temperature, which was applied to guide the preparation of the crack-free zirconium hydride. The hydriding of Zr–1 wt.%Nb alloys was carried out and the crack-free zirconium hydrides with hydrogen concentration of 1.6H/Zr (at.) and 1.8H/Zr were prepared respectively based on the calculated results.

1. Introduction

Zirconium hydride in solid state with high hydrogen concentration ($(H/Zr)_{at.} > 1.5$), low thermal neutron absorption cross section and good mechanical properties in elevated temperature, is one of the most ideal moderators for space nuclear reactors [1].

At present the preparation of bulk zirconium hydride moderator is to hydrogenate the zirconium alloys in the gas atmosphere directly. During the hydriding process, the phase of the zirconium alloys transforms from solid solution to hydride [2,3] as the hydrogen concentration increases. The transition stress in the alloys greatly damages the plastic nature of the material [4]. In addition, the δ, ε zirconium hydrides are brittle materials. So, cracking easily occurs in the hydriding process [5]. Therefore, the understanding of thermodynamic properties and phase transition behaviors is a key factor in solving the cracking problem in the preparation of bulk zirconium hydride.

Niobium is an important alloying element for the Zr-based functional materials. In this work, a thermodynamic modeling of the Zr–H–Nb system was constructed based on the Zr–Nb, Zr–H and Nb–H three binary sub-systems using CALPHAD method. The thermodynamic properties and the equilibrium phase information on the Zr-rich side (wt.%Nb $\leqslant$ 2.5) of the Zr–H–Nb system were predicted to guide the preparation of the crack-free zirconium hydride.

2. Literature review

2.1. The binary systems

The Zr–Nb binary system [6,7] consists of the gas, liquid, the terminal solid solution hcp_A3 (αZr) and bcc_A2 (βZr and βNb solid solution). Fernández Guillermet [8] established the thermodynamic modeling of Zr–Nb system. The calculated phase diagram (Fig. 1) was in good agreement with experimental data. In this work, the thermodynamic parameters assessed by A. Fernández Guillermet were adopted.

The equilibrium Zr–H binary phase diagram [9,10] is composed of the interstitial solution of H in the low temperature αZr with hcp_A3 structure, the interstitial solution of H in the high temperature βZr with bcc_A2 structure, the hypo-stoichiometric hydride fcc_C1 (δ) and the fct_L′2 hydride (ε), as well as the gas phase and liquid phase. The phase diagram of this system presents an eutectoid reaction involving α, β and δ. The phase diagram of the Zr–H system has been evaluated before. Kőnigsberger et al. [11] carried out a thermodynamic assessment of the Zr–H system without taking into account the ε phase. Dupin et al. [12] performed a optimization based on the experimental results of Moore and Young [13] and predicted the boundaries of $\delta - (\delta + \varepsilon)$ and $(\delta + \varepsilon) - \varepsilon$. The thermodynamic parameters assessed by N. Dupin were accepted in this work. The calculated Zr–H binary phase diagram is shown in Fig. 2.

The equilibrium phases of the Nb–H binary system [14] above normal temperature include gas, liquid, bcc_A2 (βNb solid solution), fco (solid solution with fc orthorhombic structure) and dihydride fcc_C1 (NbH_2). We modeled the Nb–H binary system (unpublished results) and the calculations show satisfactory agree-

* Corresponding author. Tel.: +86 10 82241302.
E-mail address: jswjw@sina.com (J. Wang).

0022-3115/$ - see front matter © 2011 Elsevier B.V. All rights reserved.
doi:10.1016/j.jnucmat.2010.12.234

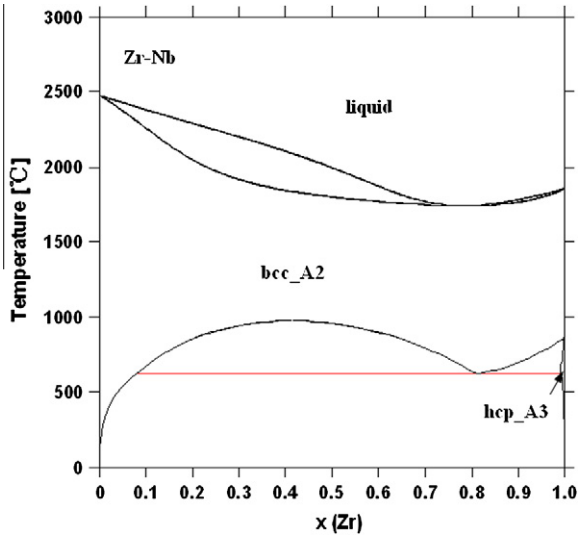

Fig. 1. Calculated Zr–Nb binary phase diagram.

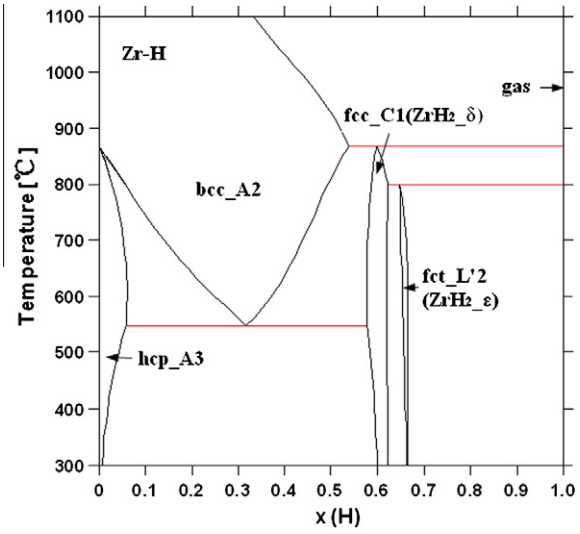

Fig. 2. Calculated Zr–H binary phase diagram.

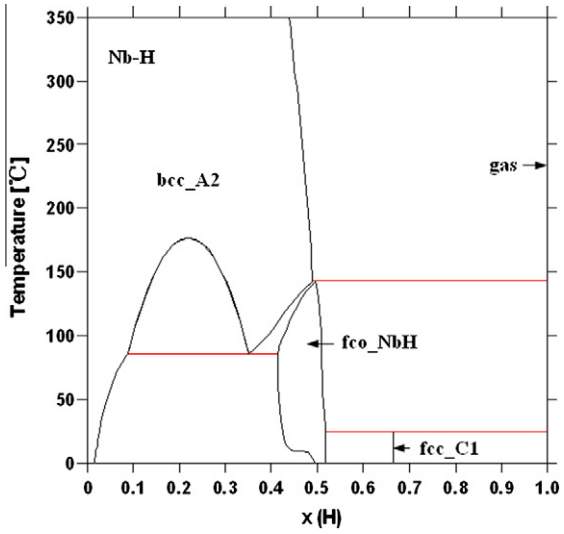

Fig. 3. Calculated Nb–H binary phase diagram.

ment with most experimental data. Fig. 3 presents the Nb–H binary phase diagram under normal pressure.

2.2. The Zr–H–Nb ternary system

The experimental thermodynamic data reported on the Zr–H–Nb system is quite limited. The pressure-composition isotherms of Zr–H–Nb system were investigated by Sinha and Singh [15–17], in whose studies the temperature ranged from 300 °C to 950 °C, the concentration scope of Nb was 2.5–20 wt.% and the hydrogen pressure detected from about 0 to 101.325 kPa. The phase boundaries of (bcc + fcc) were proposed by Sinha et al. No information about the ternary compounds of the Zr–H–Nb system was reported.

3. Extrapolation of the ternary system

The thermodynamic properties of the multi-component systems can be predicted by extrapolation, when available experimental data is not sufficient. Most methods of extrapolating the thermodynamic properties of alloys into multi-component systems are based on the summation of the binary and ternary excess parameters. The formulae for doing this are based on various geometrical weightings of the mole fractions [18].

The Muggianu's equation, developed by Muggianu et al. [19] and widely applied at present, was used to extrapolate the ternary system in this work. The excess energy G^{ex}_{mix} of a phase Φ in a ternary system based on the three binary sub-systems expands for a sub-regular solution, which is available for the Zr–H–Nb ternary system, as given by

$$\begin{aligned} G^{ex}_{mix} = {} & x_{Zr}x_{Nb}\left\{L^0_{Zr,Nb} + L^1_{Zr,Nb}(x_{Zr} - x_{Nb})\right\} \\ & + x_{Zr}x_{H}\left\{L^0_{Zr,H} + L^1_{Zr,H}(x_{Zr} - x_{H})\right\} \\ & + x_{Nb}x_{H}\left\{L^0_{Nb,H} + L^1_{Nb,H}(x_{Nb} - x_{H})\right\} \end{aligned} \quad (1)$$

where L is interaction parameter which has been taken as temperature dependent:

$$L = a + bT + cT\ln T \quad (2)$$

in which a, b, c are coefficients optimized in the binary models. The descriptions of Zr–Nb, Zr–H, Nb–H three binary systems are extrapolated at present to construct the thermodynamic modeling of Zr–H–Nb ternary system on the Zr-rich side.

4. Thermodynamic modeling

The description of the Gibbs free energy of a phase Φ is based on the following expression:

$$G^{\phi} = {}^{ref}G^{\phi} + {}^{id}G^{\phi} + {}^{ex}G^{\phi} \quad (3)$$

where ${}^{ref}G^{\phi}$ is the contribution of pure components to the Gibbs energy, ${}^{id}G^{\phi}$ is the ideal mixing contribution and ${}^{ex}G^{\phi}$ is excess Gibbs energy of mixing.

The pure solid elements in their stable phases at 298.15 K chosen as reference state for the system (SER, Standard Element Reference) are recommended by SGTE (Scientific Group Thermodata Europe), except where otherwise specified. The thermodynamic functions of pure elements (lattice stabilities) were taken from the database compiled by Dinsdale [20], excluding the H element of the liquid phase cited from Ref. [21].

The Gibbs energy functions of pure elements are given by

$${}^{0}G^{\varphi}_{i} = G^{\varphi}_{i} - H^{SER}_{i} = a + bT + cT\ln T + dT^2 + eT^3 + fT^{-1} + hT^{-9} \quad (4)$$

where a–h are coefficients.

4.1. The gas phase

The gas phase containing H, H_2, Nb, Zr, Zr_2 species was considered as an ideal mixture. The molar Gibbs energy of the gas phase is then given by

$$G^{gas} = \sum_i x_i \left[{}^0G_i^{gas} + RT\ln(P/P_0) \right] + RT\sum_i x_i \ln x_i \tag{5}$$

where ${}^0G_i^{gas}$ is the standard Gibbs energy of the component i in the gas state, P_0 is the standard pressure of 101.325 kPa, x_i is the mole fraction of species i and R is the gas constant. Diatomic H_2 is the dominant species, while the others have practically zero amounts.

4.2. The liquid phase

The liquid phase are modeled by the substitutional solution model and the Gibbs energy is described as

$$\begin{aligned} {}^{ref}G^{liq} &= x_H G_H^{liq} + x_{Nb} G_{Nb}^{liq} + x_{Zr} G_{Zr}^{liq} \\ {}^{id}G^{liq} &= RT[x_H \ln x_H + x_{Nb} \ln x_{Nb} + x_{Zr} \ln x_{Zr}] \\ {}^{ex}G^{liq} &= x_H x_{Nb} \sum_v {}^vL^{liq}_{H,Nb}(x_H - x_{Nb})^v + x_H x_{Zr} \sum_v {}^vL^{liq}_{H,Zr}(x_H - x_{Zr})^v \\ &\quad + x_{Nb} x_{Zr} \sum_v {}^vL^{liq}_{Nb,Zr}(x_{Nb} - x_{Zr})^v \end{aligned} \tag{6}$$

where v is the order of the term considered.

4.3. The hcp_A3, bcc_A2 and fcc_C1 phases

The solid solutions of hcp_A3, bcc_A2 are described by the two sublattice model $(Nb, Zr)_a(H, Va)_b$. We assumed the two fcc_C1 hydrides ZrH_2 and NbH_2 inter-dissolve infinitely on the Zr-rich side, and described the fcc_C1 phase as the two sublattice model $(Nb, Zr)_a(H, Va)_b$. The Gibbs energy of these phases is described as follows:

$$\begin{aligned} {}^{ref}G^{\phi} &= y'_{Zr}y''_H {}^0G^{\phi}_{Zr:H} + y'_{Nb}y''_H {}^0G^{\phi}_{Nb:H} + y'_{Zr}y'_{Va} {}^0G^{\phi}_{Zr:Va} + y'_{Nb}y''_{Va} {}^0G^{\phi}_{Nb:Va} \\ {}^{id}G^{\phi} &= RT[a(y'_{Zr}\ln y'_{Zr} + y'_{Nb}\ln y'_{Nb}) + b(y''_H \ln y''_H + y''_{Va}\ln y''_{Va})] \\ {}^{ex}G^{\phi} &= y'_{Zr}y'_{Nb}(y''_H L^{\phi}_{Zr,Nb:H} + y''_{Va}L^{\phi}_{Zr,Nb:Va}) + y''_H y''_{Va}(y'_{Zr}L^{\phi}_{Zr:H,Va} + y'_{Nb}L^{\phi}_{Nb:H,Va}) \end{aligned} \tag{7}$$

where ${}^0G^{\phi}_{Zr:H}$, ${}^0G^{\phi}_{Nb:H}$, ${}^0G^{\phi}_{Zr:Va}$, ${}^0G^{\phi}_{Nb:Va}$ are the Gibbs energy of the "end-members", y'_i is the site fraction of component i in the first sublattice, y''_i is the site fraction of component i in the second sublattice, a and b denote the number of sites in each sublattice and present the mole ratio between sublattices. For hcp_A3, $a = 1$, $b = 1$; for bcc_A2, $a = 1$, $b = 3$; for fcc_C1, $a = 1$, $b = 2$. More detailed description of the sublattice model can be found in Ref. [22].

4.4. The fco and fct_L′2 phases

fco and fct_L′2 phases treated individually are taken from the binary Nb–H [14] and Zr–H [12] sub-systems, respectively. According to the structural characters, the fco phase is described as two sublattice model (Nb, Va)(H, Va) and the fct_L′2 phase is described as $(Zr)(H,Va)_2$. The Gibbs energy of fco phase is given by

$$\begin{aligned} {}^{ref}G^{\beta} &= y'_{Nb}y''_H {}^0G^{\beta}_{Nb:H} + y'_{Nb}y''_{Va} {}^0G^{\beta}_{Nb:Va} \\ {}^{id}G^{\beta} &= RT\left[(y''_{Nb}\ln y''_{Nb} + y'_{Va}\ln y'_{Va}) + (y''_H \ln y''_H + y''_{Va}\ln y''_{Va})\right] \\ {}^{ex}G^{\beta} &= y'_{Nb}y''_H y''_{Va}\left[L^{0,\beta}_{Nb:H,Va} + L^{1,\beta}_{Nb:H,Va}(y''_H - y''_{Va})\right] \\ &\quad + y'_{Nb}y'_{Va}y''_H L^{0,\beta}_{Nb,Va:H} \end{aligned} \tag{8}$$

And the Gibbs energy of fct_L′2 phase is described as

$$\begin{aligned} {}^{ref}G^{\varphi} &= y'_{Zr}y''_H {}^0G^{\varphi}_{Zr:H} + y'_{Zr}y''_{Va} {}^0G^{\varphi}_{Zr:Va} \\ {}^{id}G^{\varphi} &= 2RT(y''_H \ln y''_H + y''_{Va}\ln y''_{Va}) \\ {}^{ex}G^{\varphi} &= y''_H y''_{Va} L^{\varphi}_{Zr:H,Va} \end{aligned} \tag{9}$$

5. Results and discussion

Fig. 4 shows the calculated pressure-composition isotherms of the Zr–H–Nb system (wt.%Nb = 2.5) at different temperatures. The experimental results by Sinha and Singh [15] are superimposed as data points for comparison. In the isotherms, where the pressure is composition-dependent, a single solid phase exists; on the plateaus, where the pressure is independent of composition, two solid hydride phases are in equilibrium. The phase field boundary composition data, hydrogen equilibrium pressure for the two-phase (bcc + fcc) region and the isobaric limit can be defined from the isotherms, which is shown in Table 1. In general, the agreement between calculated and experimental data is satisfactory.

The hydrogen composition in the Zr–H–Nb equilibrium system is determined by the temperature and hydrogen pressure. Fig. 5 presents the relation between equilibrium hydrogen composition and temperature in the Zr–H–Nb system (wt.%Nb = 1) at 101.325 kPa. A rule of correspondence between hydrogen concentration $(H/Zr)_{at.}$ and temperature is concluded from the curve. As the temperature decreases, the hydrogen composition increases and the equilibrium phases of the system also change, which is shown in Fig. 4.

Generally, the preparation of the crack-free zirconium hydride is an isopiestic hydriding process. However, control of the changing rate of temperature is the key factor in preventing the material from cracking. Higher cooling rate favors fast hydrogen absorption of zirconium alloy, even faster during the phase transitions, which accelerates the volume expansion and accumulates the stress inside the alloy. In this case, the internal stress tends to release in the shape of crack during the phase transitions of bcc ↔ bcc + fcc and fcc ↔ fcc + fct. So the phase transition temperatures are important for the settings of experimental conditions.

Wherefore, some equilibrium phase information of the Zr–H–Nb system (wt.%Nb = 1, P_{H_2}=101.325 kPa) is concluded from Fig. 4 as follow. The zirconium hydride with hydrogen concentration of 1.8H/Zr in atom ratio is fct structure in equilibrium at 788 °C,

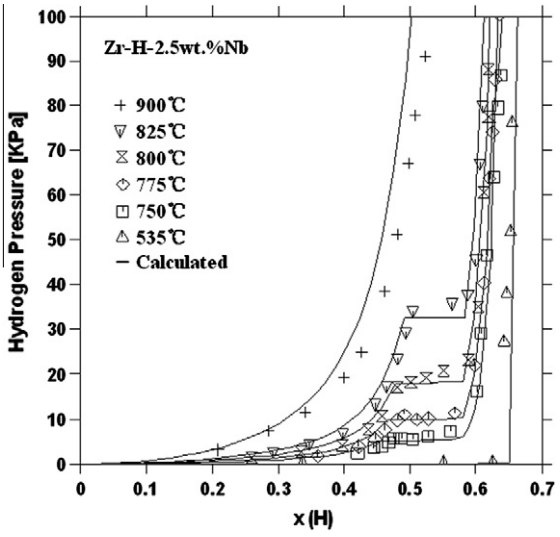

Fig. 4. Calculated pressure-composition isotherms of the Zr–H–Nb system (wt.%Nb = 2.5). Experimental points from Ref. [15].

Table 1
Calculated composition limits in the Zr–H–Nb system (wt.%Nb = 2.5).

T (°C)	Composition in the (bcc + fcc) region (at.%H)		Equilibrium hydrogen pressure in the (bcc + fcc) region (kPa)		Isobaric limit for P_{H_2}=101.325 kPa (at.%H)	
	Calculated	Sinha and Singh [15]	Calculated	Sinha and Singh [15]	Calculated	Sinha and Singh [15]
700	42.4–54.0	44.9–54.8	1.520	1.560	65.59	65.06
750	45.2–54.5	47.6–55.8	5.533	6.093	63.2	64.3
775	46.6–56.3	48.2–56.4	10.252	10.786	63.9	63.8
800	47.8–56.9	49.1–57.1	18.478	19.998	62.1	62.9
825	49.2–57.9	51.0–57.7	32.971	37.197	61.3	61.7
850	52.7–58.6	53.2–57.6	59.702	60.328	60.2	60.4

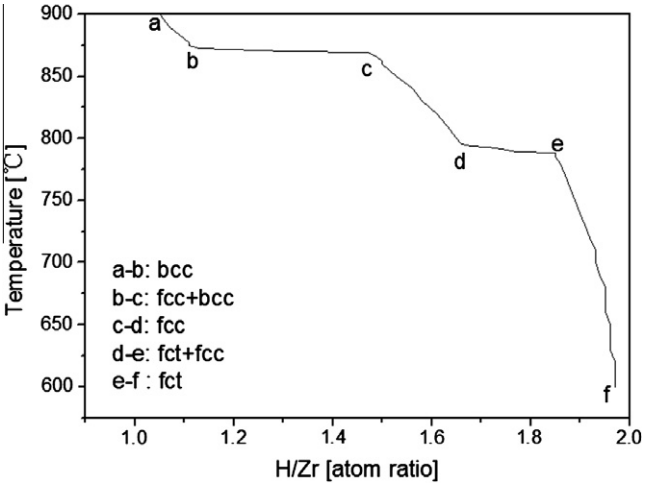

Fig. 5. Calculated equilibrium hydrogen composition and phase change with temperature in the Zr–H–Nb system (wt.%Nb = 1).

and the zirconium hydride with 1.6H/Zr is fcc structure at 820 °C. The phase transition temperature of bcc ↔ bcc + fcc is 872 °C, while that of fcc ↔ fcc + fct is at 794 °C.

6. Experiment and analysis

6.1. Experiment

The hydriding experiments for Zr–1 wt.%Nb alloy were carried out in this work. The alloys were prepared with reactor grade zirconium and 99.9% purity niobium using arc melting method, and annealed in vacuum at 1500 °C for 48 h to ensure homogeneity. Samples used for hydriding experiments were 20–40 mm in diameter and 5–20 mm in length. The samples were chemical polished for 30 s in the solution of 10%HF–40%HNO_3–50%H_2O (volume fraction) in order to remove the nature oxide on the surface.

The hydriding experiments were carried out in the modified Sieverts apparatus. The apparatus was vacuumized to 2×10^{-3} Pa and then heated in 10 °C/s to an appropriate temperature. Hydrogen with the initial purity of 99.9999% was further purified by passing through a hot titanium bed, before it was transferred into the apparatus. The pressure inside the apparatus was programmed below 105 kPa and the hydrogen flow rate kept constant at a relatively low level.

Figs. 6 and 7 shows the experimental temperature curve which including 5 steps (A–B, B–C, C–D, D–E, E–F). Table 2 presents the contributions of each heating step in the hydriding process. At the end of the heating program, hydriding process was stopped by removing the rest hydrogen in apparatus. The as-prepared hydrides were cooled down to room temperature naturally.

According to the calculated results, the zirconium hydride with 1.8H/Zr is characterized by the fct phase at 788 °C in equilibrium,

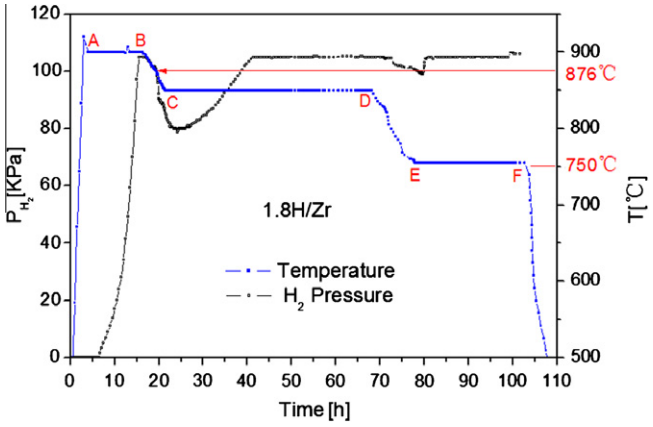

Fig. 6. Experimental curve for zirconium hydride with 1.8H/Zr (at.).

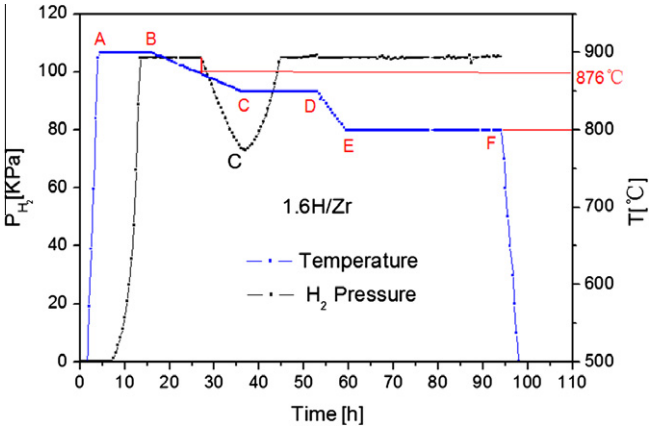

Fig. 7. Experimental curve for zirconium hydride with 1.6H/Zr (at.).

Table 2
Instruction for the experimental temperature curve.

Step	Heating mode	Contribution
A–B	Constant temperature	Absorb hydrogen for the solid solution at high temperature (~900 °C)
B–C	Temperature drops slowly	Avoid cracking for bcc ↔ bcc + fcc transition
C–D	Constant temperature	Absorb hydrogen for the fcc single phase
D–E	Temperature drops slowly	Avoid cracking for fcc ↔ fcc + fct transition
E–F	Constant temperature	Determine the hydrogen concentration of the zirconium hydride

while the equilibrium phase of zirconium hydride with 1.6H/Zr is fcc at 820 °C. With view for the hydrogen loss of the samples after

the hydriding process, the temperatures in the last step (E–F) were adjusted to 750 °C for 1.8H/Zr zirconium hydride and 800 °C for 1.6H/Zr hydride.

6.2. Experimental analysis

In the first step A–B, The alloys absorbed hydrogen at 900 °C and the hydrogen concentration tended towards saturation at the end of A–B. To avoid the zirconium alloys absorb hydrogen too fast, the temperature dropped slowly around 872 °C in step B–C for the phase transition of bcc ↔ bcc + fcc according to the calculated results. An obvious decline of hydrogen pressure is observed in Figs. 6 and 7, which mainly caused by the bcc ↔ bcc + fcc transition. Analogously, when the temperature reached about 795 °C, the fcc zirconium hydride transformed to fct zirconium hydride for higher hydrogen level, which created another decline of hydrogen pressure in step D–E (Fig. 6). The temperatures are controlled to drop in a slow rate during the steps of B–C and D–E corresponding to the two-phase transitions, which makes the alloys absorb hydrogen slowly and leads the stress inside the alloys release by other means instead of crack. These two steps of B–C and D–E play the decisive role for the inhibition of crack in the preparation of zirconium hydride. The second decline peak is not observed in Fig. 4 (for 1.6H/Zr), which is because of the hydriding temperature in this experiment (800 °C in minimum) did not reach the fcc ↔ fcc + fct phase transition temperature (795 °C).

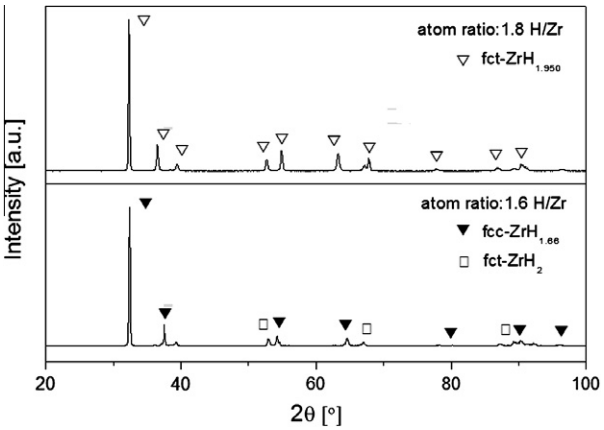

Fig. 8. XRD patterns of zirconium hydride samples.

Fig. 9. Images and micrograph on surface of the crack-free zirconium hydride samples.

The crack-free zirconium hydride samples with hydrogen concentration of 1.8H/Zr and 1.6H/Zr were prepared from the experiments. Fig. 9 shows the images of crack-free samples and its micrograph on surface is observed by optical microscope. The surface of the zirconium hydride samples is flat and no visible cracks can be seen in appearance. The phase identification of the samples was performed on a Rigaku D/max-2500 diffractometer (45 kV/250 mA) with a graphite monochrometer from Fig. 8. The sample with 1.8H/Zr is composed of fct zirconium hydride and the main phase of zirconium hydride with 1.6H/Zr is fcc. A little amount of fct zirconium hydride is detected in the sample with 1.6H/Zr, which was probably produced around the fcc ↔ fcc + fct phase transition temperature during cooling process after the hydriding.

7. Conclusion

(1) The Zr–H–Nb ternary thermodynamic modeling of the Zr–H–Nb ternary system on the Zr-rich side (wt.%Nb ⩽ 2.5) was constructed by the Muggianu scheme. The calculated results show a good agreement with the experimental data.
(2) Some thermodynamic information of the Zr–H–Nb system (wt.%Nb = 1, P_{H_2}=101.325 kPa) was calculated to guide the preparation of the crack-free zirconium hydride. The zirconium hydride with hydrogen concentration of 1.8H/Zr in atom ratio is fct structure in equilibrium at 788 °C, and the zirconium hydride with 1.6H/Zr is fcc structure at 820 °C. The phase transition temperature of bcc ↔ bcc + fcc is 872 °C, while that of fcc ↔ fcc + fct is at 794 °C.
(3) The corresponding hydrogenations for Zr–1Nb alloys were carried out according to the calculated results. Control of the changing rate of temperature during the phase transition of bcc ↔ bcc + fcc and fcc ↔ fcc + fct is the key factor in preventing the material from cracking. The crack-free zirconium hydrides were prepared and the experimental results agree well with the calculated prediction.
(4) With the thermodynamic description available, one can now make various calculations of practical interest.

Acknowledgements

Financial support from the National Natural Science Foundation of China is gratefully acknowledged (Grant No. 50674015).

References

[1] M.S. El-Genk, D. Paramonov, J. Nucl. Saf. 35 (1994) 74–85.
[2] K. Konashi, T. Ikeshoji, Y. Kawazoe, Alloys Compd. 356–357 (2003) 279–282.
[3] N.N. Ponomarev-Stepnoi, V.G. Bubelev, Y.S. Glushkov, J. Nucl. Sci. Eng. 119 (1995) 108–115.
[4] U. Zander, D. Koeter, Mater. Sci. Eng. A A294–A296 (2002) 112–115.
[5] B. Tsuchiya, M. Teshigawara, K. Konashi, J. Alloys Compd. 330–332 (2002) 357–360.
[6] J.P. Abriata, J.C. Bolcich, Bull. Alloy Phase Diag. 3 (1982) 34–44.
[7] H. Okamoto, J. Phase Equilib. 13 (1992) 577.
[8] A. Fernández Guillermet, Z. Metallkd 82 (1991) 478–487.
[9] E. Zuzek, J.P. Abriata, in: F.D. Manchester (Ed.), Phase Diag. Binary Hydrogen Alloys, ASM International, Materials Park, OH, 2000, pp. 309–322.
[10] H. Okamoto, J. Phase Equilib. Diffus. 27 (2006) 548–549.
[11] E. Königsberger, G. Eriksson, W.A. Oates, J. Alloys Compd. 299 (2000) 148–152.
[12] N. Dupin, I. Ansara, C. Servant, J. Nucl. Mater. 275 (1999) 287–295.
[13] K.E. Moore, W.A. Young, J. Nucl. Mater. 27 (1968) 316–324.

[14] J.F. Smith, Bull. Alloy Phase Diag. 4 (1983) 39–46.
[15] V.K. Sinha, K.P. Singh, J. Nucl. Mater. 36 (1970) 211–217.
[16] V.K. Sinha, K.P. Singh, Metall. Trans. 3 (1972) 1581–1585.
[17] V.K. Sinha, Metall. Trans. A 7A (1976) 472–475.
[18] N. Saunders, A.P. Miodownik, in: R.W. Cahn (Ed.), CALPHAD (Calculation of Phase Diagrams): A Comprehensive Guide, Pergamon press, New York, 1998.
[19] Y.M. Muggianu, M. Gambino, J.P. Bros, J. Chim. Phys. 72 (1975) 83–88.
[20] A.T. Dinsdale, Calphad 15 (1991) 317–425.
[21] C. Qiu, S.M. Opalka, G.B. Olson, D.L. Anton, Int. J. Mater. Res. 97 (2006) 1484–1494.
[22] I. Ansara, N. Dupin, H.L. Lukas, B. Sundman, in: P. Nash, B. Sundman (Eds.), Proc of TMS Conf. on Applications of Thermodynamics in the Synthesis and Processing of Materials, Warrendale, PA, USA, 1995, pp. 273–283.